A Novel Method to Obtain Modulus Image of Soft Tissues Using Ultrasound Water Jet Indentation: A Phantom Study

Min-Hua Lu, *Member, IEEE*, Yong-Ping Zheng*, *Senior Member, IEEE*, and Qing-Hua Huang, *Member, IEEE*

***Abstract*—The alteration of tissue stiffness is generally known to be associated with pathological changes. Ultrasound indentation is one of the methods that can be used to assess the mechanical properties of the soft tissues. It uses a flat-ended ultrasound transducer to directly contact the tissue to sense tissue deformation under an applied load. This paper introduced a novel noncontact ultrasound indentation system using water jet compression. The key idea was to utilize a water jet as the indenter as well as the coupling medium for propagation of the ultrasound beam. High frequency focused ultrasound (20 MHz) was used to measure the indentation deformation at a microscopic level. It has been demonstrated that the system could effectively assess the tissue-mimic phantoms with different stiffness. Water jet coupling allows the system to conduct C-scan on soft tissues rapidly and conveniently. By applying different pressures while taking C-scan sequences, the modulus images of the phantoms could be obtained based on the applied pressure and the phantom deformation and thickness. This paper presented the preliminary results on gel phantoms. The spatial resolution, the contrast resolution of the measurements and the reproducibility of the results were also discussed.**

***Index Terms*—Articular cartilage, elasticity imaging, elastography, elastomicroscopy, high-frequency ultrasound, modulus image, tissue, ultrasound indentation, water jet.**

I. Introduction

TISSUE stiffness is generally known to be associated with pathological changes, such as sclerous cancer, edema, degeneration, fibrosis and pressure sore [1], [2]. The changes of tissue stiffness are caused either by exudation of fluids from the vascular system into the extra- or intracellular space or by the loss of lymphatic systems, as in the case of cancer tumors. Normal tissues may also have different stiffness, which is important information for tissue characterization. The mechanical properties of tissues may have different values depending on whether they are measured *in vivo* or *in vitro* and *in situ* or as an excised specimen [3], [4].

Indentation is one of the most frequently used approaches to assess the soft tissues *in situ* or *in vivo*. Cylindrical flat-ended or spherical indenters have been used to perform contact loading on soft tissues. By obtaining tissue thickness using a needle probe or optical based methods, researchers have reported mathematical solutions to extract the elastic modulus of thin layer soft tissues from indentation data [5]–[12]. Ultrasound indentation was proposed in the last decade which integrated a load cell and a flat-ended unfocused ultrasound transducer to monitor the indentation response of soft tissues [13]–[20]. The ultrasound transducer served as an indenter to compress the tissue and meanwhile collected the echoes reflected from the tissues during indentation to obtain the deformation and tissue thickness simultaneously and noninvasively. Ultrasound indentation has been widely used to assess soft tissues *in vivo*, such as normal limb tissues [21], [22], residual limb tissues [23], diabetic foot tissues [15], [24], fibrotic neck tissues induced by radiotherapy [25]–[27], breast tissues [20], spinal tissues [28], and articular cartilage [18], [19]. Ultrasound indentation typically operates in the frequency range between 2 and 10 MHz and is normally used to measure the mechanical properties of entire tissue layers. Its resolution is not sufficient to map the mechanical properties of soft tissue with fine structures, such as articular cartilage [29], corneal tissues [30] or skins [31]. Using high-frequency for ultrasound indentation may improve the resolution. However, the high-frequency focused ultrasound transducer cannot be used for traditional contact indentation due to its concave-face. In addition, it is not common to use contact indentation to image the distribution of elastic modulus for a region of tissue due to the restrictions of the low spatial resolution (typically greater than 2 mm) and the long measurement time [32], [33]. With the use of nanoindentation [34], high resolution modulus imaging can be achieved for a small region of a thin layer of material which is likely to be homogeneous in the entire thickness. However, the technique has not been widely used for the assessment of soft tissue as the testing results are highly dependent on the surface condition of the specimen [35].

Ultrasound elastography, on the other hand, can provide a local strain image inside soft tissues along the transducer axis by comparing the ultrasound cross section images before and after compression [36]–[38]. The local strain image with good resolution and contrast is useful for medical diagnosis. The medical applications of ultrasound elastography technique range from tumor detection [2] to the study of skeletal muscle contraction [39], from the assessment of vascular health [40] to the renal transplant rejection [41]. However, tissue strain is not a fundamental tissue property as it depends on the tissue mechanical properties and other factors, such as the tissue geometry, tissue

Manuscript received October 6, 2005; revised May 21, 2006. This work was supported in part by the Research Grants Council of Hong Kong under Grant PolyU 5245/03E and Grant PolyU 5318/05E and in part by the Hong Kong Polytechnic University. *Asterisk indicates corresponding author.*

M.-H. Lu and Q.-H Huang are with the Department of Health Technology and Informatics, The Hong Kong Polytechnic University, Hong Kong, China (e-mail: minhua.lu@polyu.edu.hk; rchqh@inet.polyu.edu.hk).

*Y.-P. Zheng is with the Department of Health Technology and Informatics, The Hong Kong Polytechnic University, Hong Kong, China (e-mail: ypzheng@ieee.org).

Digital Object Identifier 10.1109/TBME.2006.884646

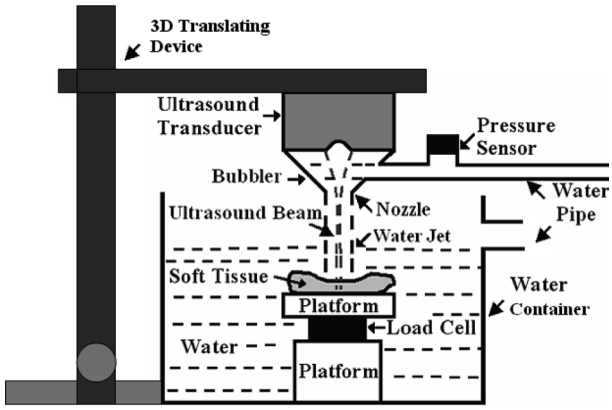

Fig. 1. Diagram of ultrasound indentation system using the water jet compression. The water jet was used as an indenter and focused high-frequency ultrasound was employed to monitor the deformation of the soft tissue. The 3-D translating device facilitated the system to conduct C-scan for the soft tissue. By applying different pressure for C-scan sequences, the modulus image was obtained with the recorded pressure, deformation and thickness.

connectivity, modulus contrast and distribution, applied strain and boundary conditions. Shear modulus images of soft tissues were obtained when the tissue was vibrated either by a low-frequency shear wave produced by an external vibrator [42]–[45] or by the acoustic radiation force produced by focused ultrasound [46]–[48]. The spatial resolution of the elasticity images using the current medical ultrasound frequency is usually on the order of several millimeters and may not be sufficient for the assessment of tissues with fine structures.

Ultrasound C-scan imaging provides a useful view of an object, showing a plane perpendicular to the ultrasound beam. It has been widely used in the aerospace industry to detect the surface corrosion, delaminations, voids, cracks and other faults in aging aircraft [49], [50]. In this paper, we introduced a new ultrasound water indentation system, which used a water beam as the indenter as well as the medium for ultrasound propagation. High-frequency ultrasound was utilized to measure the indentation deformation at a microscopic level. It had been demonstrated in a preliminary study that the water jet ultrasound indentation system could effectively differentiate phantoms with different stiffness [51]. In this study, we extended our work to C-scan imaging. By applying different water pressures for C-scan sequences, the modulus image could be obtained. The system development and experimental protocol were introduced. The experimental results on gel phantoms and discussion of the results were also provided.

II. Methodology

A. Ultrasound Water Indentation System

A noncontact ultrasound indentation system was constructed using a water jet as an indenter. As shown in Fig. 1, a bubbler was used to eject a water jet by controlling the water flow. The diameter of the water ejecting nozzle was 1.94 mm. A 20-MHz focused ultrasound transducer (GE Panametrics, Inc., OH) was fixed with the bubbler, *i.e.*, the water ejector. The focused ultrasound beam could propagate through the bubbler when it was full of water as the coupling medium. The transducer and the bubbler were installed to a 3-D translating device (Parker Hannifin Corporation, Irvine, CA) which was used to adjust the distance between the nozzle and the specimen surface and to perform the 2-D scanning over a tissue specimen or phantom. For the tests reported in this study, the distances from the specimen surface to the nozzle outlet and the transducer surface were adjusted to be 5.0 and 19.5 mm, respectively. The phantom was placed on a rigid platform within a water container. An outlet on one side of the container was used to control the water level. A pressure sensor (EPB-C12, Entran Devices, Inc., Fairfield, NJ) was used to measure the water pressure within the water pipe. A load cell (ELFS-T3M, Entran Devices, Inc.) located under the platform could monitor the overall force applied on the phantom. By calibrating the relationship between the overall force applied on the load cell and the pressure within the water pipe for the central region of the phantom, the stress applied on the phantom could be calculated using the water pressure measured by the pressure sensor [51]. A program was developed using Microsoft VC++ to control the three-dimensional (3-D) translating device and to collect, process and display the ultrasound signals, together with the force and the pressure values, in real time during the indentation process. Thus, the movement of the transducer and the acquisition of the radio frequency ultrasound signal, force or pressure data were synchronized. The ultrasound echoes reflected from the phantom surface and bottom under different loading conditions were tracked using a cross-correlation algorithm [31]. During tracking, the two echoes of one typical A-mode ultrasound signal were selected by two pairs of cursors. The cross-correlation was then used to search the corresponding echoes in other A-mode signals of the whole two-dimensional scan under the same loading condition. After that, the same pairs of echoes were used to search another set of the A-mode signals obtained under a different loading condition. The deflection of the time of flight of the echoes obtained from the same location was, thus, obtained. The original tissue thickness and the subsequent change of thickness, i.e., the deformation of the tissue under indentation, were derived from the time information. The modulus was calculated from the water pressure and the local strain, which was calculated from the local deformation and thickness.

B. Phantom Fabrication

Six pieces of tissue-mimicking phantom with a diameter of 25 mm and a height of 5 mm were prepared for the experiments (Fig. 2). Each consisted of a stiff cylindrical inclusion with a diameter of 8 mm inside a homogeneous background. This axisymmetric cylindrical geometry was chosen as an approximation of the cross section of a hard cancerous and noncancerous inclusion inside soft tissue [2]. The stiff inclusion cylinders were made of silicones (Rhodia RTV 573, Rhodia Inc. CN7500, Cranbury, NJ, Wacker M4648 and M4600, Wacker Chemicals Hong Kong Ltd., Hong Kong, China). The backgrounds were made of agar-water mixture with different concentrations of agar, ranging from 10.0 to 30.0 g/L. To produce a homogeneous background, the agar powder (Fisher Scientific Co. Fairlawn, NJ) was hydrated with a solution of deionized water and n-propanol and heated to 70 °C to disperse the colloid, clarify the solution, and release the trapped gasses. When the mixture was cooled to 30 °C (near its congealing point), a

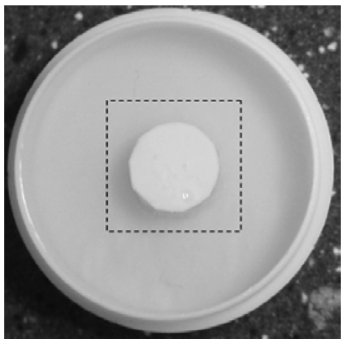

Fig. 2. A picture of the cylindrical phantom used in this study. Its diameter was 25 mm, and the central square region (12 mm × 12 mm) was tested. The inclusion with a diameter of 8 mm was made of different silicones and background was made of agar-water mixture with different concentrations.

TABLE I
DESCRIPTION OF THE PHANTOMS USED IN THIS STUDY

Phantom	Background # (Agar weighted concentration, g/L)	Inclusion (Silicone *)	Modulus Contrast** (dB)
CP1	10	RTV 573	10.02
CP2	15	RTV 573	8.78
CP3	15	M4648	7.05
CP4	20	RTV 573	4.97
CP5	20	M4600	3.38
CP6	30	M4600	0.97

The background gel phantom was made of agar powder hydrated with a solution of deionized water. N-propanol and formaldehyde were added with weighted concentrations of 8.02% and 0.05‰, respectively.
* The silicones used for the inclusion cylinders were Rhodia RTV 573 and Wacker M4648 and M4600.
** The modulus contrast was defined as the ratio of the compressive Young's modulus of the inclusion to that of the background material, which was measured using the uniaxial compression test.

small quantity of formaldehyde (Fisher Scientific Co. Fairlawn, NJ) was added to raise the melting point of the congealing point of the congealed gel [52]. A total of six phantoms labeled as CP1 to CP6 were made and used for the C-scans. Table I shows the descriptions of the gel samples used in this study.

In addition, uniform cylindrical samples with the same dimension as the mixed phantoms but without inclusion were also prepared for each phantom material. Their Young's moduli were measured using uniaxial compression tests with a material testing machine [51]. Typically, samples were preloaded to 2% and then compressed to an additional 5%. The interfaces between the sample and the compressor and the plate were lubricated by oil to avoid frictions. All the measurements were performed at room temperature $(20.5\,^{\circ}\mathrm{C} \pm 0.5\,^{\circ}\mathrm{C})$.

C. C-Scan Experiments

During the scan experiment, the phantom was placed on the specimen platform and fixed to avoid the slip. An area of 12 mm × 12 mm was scanned along both directions with a step of 0.2 mm. The scan area was selected based on the boundary requirement of indentation that the lateral dimension of the sample should be at least three times larger than the diameter of the indenter [53]. The water temperature used for the water jet indentation was approximately 20 °C. The water pressure during a single C-scan was maintained to be a constant. The scan time for each phantom was at most 20 min. Typically, the phantoms were preloaded with a pressure of 3 kPa to obtain the first C-scan and were then scanned with a pressure of no more than 20 kPa for the second C-scan. The applied preloading could help to exclude the toe region in the pressure-deformation relationship so as to make the measurement result more consistent. This is a widely used procedure for the mechanical test of tissues [3]. The preloading of 3 kPa was treated as the baseline for reporting the pressure values, i.e., all the measured values of pressure were subtracted by 3 kPa. For each phantom, the maximal strain was controlled at 5%, within which level the phantoms could be normally modeled as linear elastic materials. The ultrasound pulsed echoes reflected from the sample surface and bottom were tracked for each corresponding measurement site for the 12 mm × 12 mm area to compose the strain image (60 × 60 pixels). The compressive modulus of each indentation site was calculated from the local stress and strain data with the assumption that the Poisson's ratios of the inclusion and background material were the same. The strain contrast (S_c) was defined as the ratio of the average strain of the background (S_b) to that of the inclusion (S_i)

$$S_c(dB) = 10 * \log\left(\frac{S_b}{S_i}\right). \tag{1}$$

Correspondingly, the modulus contrast (E_c) was defined as the ratio of the average modulus of the inclusion (E_i) to that of the background (E_b)

$$E_c(dB) = 10 * \log\left(\frac{E_i}{E_b}\right). \tag{2}$$

In this paper, both average moduli and modulus contrasts of the phantoms obtained using the water jet indentation method were correlated with those measured using the uniaxial compression tests. To assess the reproducibility of the modulus imaged by the ultrasound water indentation system, a repeatability test was conducted on phantom CP1. The phantom was scanned twice under the approximately same indentation level. Two modulus images were obtained from these two independent scan sequences. The cross-correlation was used to quantify the similarity between the corresponding modulus images.

III. RESULTS

Fig. 3 shows a typical stress and strain data set of a gel phantom with a 15 g/L agar weighted concentration. It is obvious that the phantom behaved as an approximately linear elastic material in this strain range. The slope of the loading portion was chosen to calculate the modulus (stress/strain) of the sample, where the stress was calculated using the force applied on the phantom surface by the water jet divided by the cross section area of the water beam, and the strain was calculated using the local deformation divided by the original thickness. Fig. 4 shows the Young's modulus of each phantom measured by the material testing machine using the uniaxial compression tests. The actual modulus contrasts for phantom CP1 to CP6 were, thus, obtained (Table I).

Fig. 5 shows the typical strain and modulus images of a phantom obtained under different indentation levels. Fig. 5(a), (b), and (c) shows the strain images and Fig. 5(d), (e), and

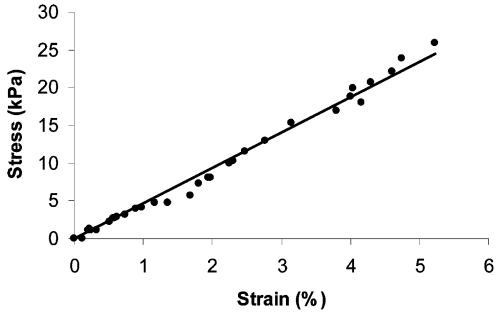

Fig. 3. A typical stress-strain curve obtained from a gel sample with a 15 g/L agar weighted concentration using water jet ultrasound indentation. The slope of the loading curve was used to calculate the modulus (stress/strain), where the stress was calculated by the force applied on the phantom surface by the water jet divided by the cross section area of the water beam, and the strain was calculated by the local deformation divided by the phantom thickness.

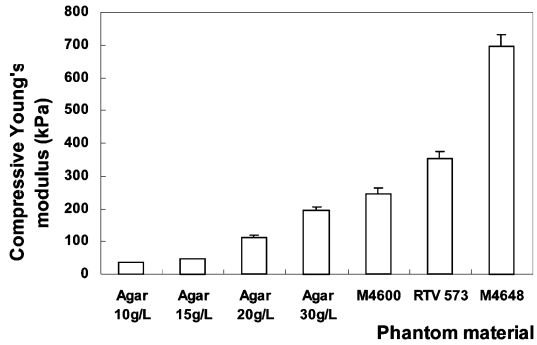

Fig. 4. The compressive Young's modulus of each phantom material which was listed in Table I. The modulus was measured by the uniaxial compression test using the material testing machine.

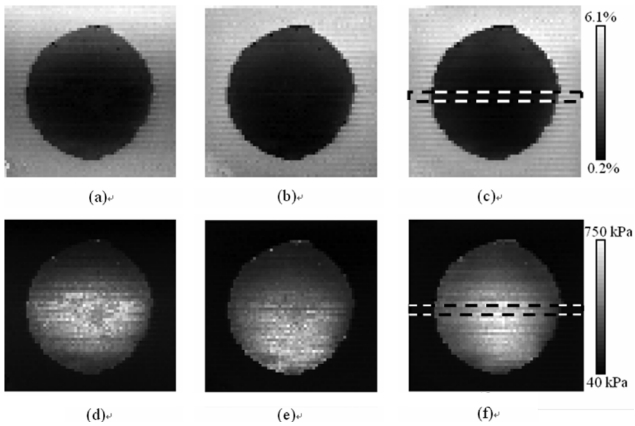

Fig. 5. Typical strain and modulus images of a phantom named CP2 with a stiffer inclusion (the diameter of the inclusion was 8 mm) obtained under different indentation levels. The scanning area was 12 mm × 12 mm with a step of 0.2 mm. (a), (b), and (c) Strain images obtained under different pressure levels, i.e., from 0 to 7.3 kPa, from 0 to 10.7 kPa, and from 0 to 15.5 kPa, respectively and (d), (e), and (f) are the corresponding modulus images. The average strains of the whole background materials were 2.0%, 2.7%, and 4.0%, respectively. The dashed rectangles indicated the regions used for the plot of strain and modulus profiles in Fig. 6.

(f) shows the corresponding modulus images obtained under different pressure levels, i.e., from 0 to 7.3 kPa, 0 to 10.7 kPa, and 0 to 15.5 kPa, respectively. The average strains of the whole background materials were 2.0%, 2.7%, and 4%, respectively. It was found that a relatively larger strain level could improve

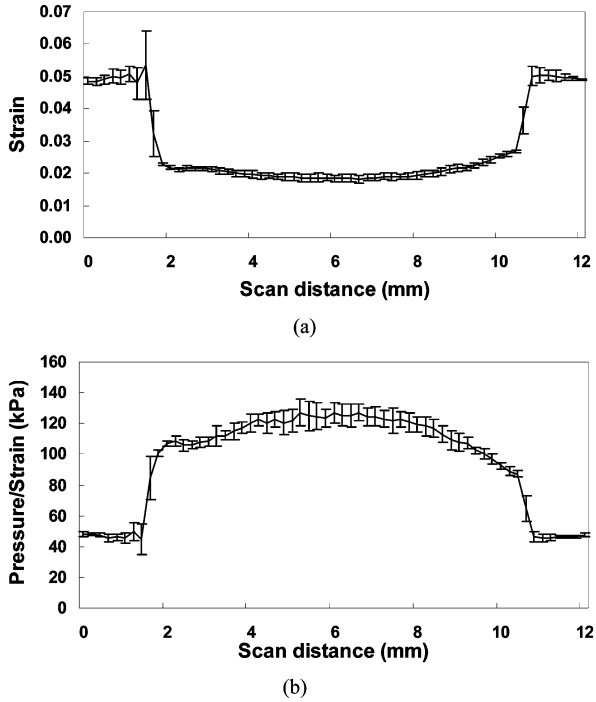

Fig. 6. (a) Average strain and (b) corresponding modulus profiles taken from the center of the strain image [Fig. 5(c)] and the corresponding modulus image [Fig. 5(f)]. The error bar indicates the strain and modulus variation across 0.6-mm-wide region around the center. The 0.6-mm-wide region was indicated by the dashed rectangles in Fig. 5. The scan distance means the horizontal distance of a measurement region with reference to the left side of the image.

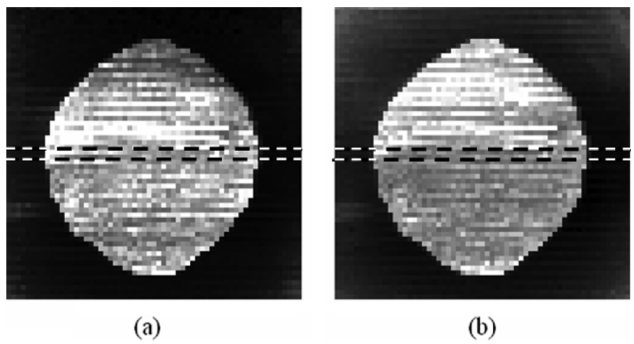

Fig. 7. The modulus images obtained from two independent scans of the same phantom under the approximately same indentation level. The resemblance of the images demonstrated the reproducibility of the modulus imaging using the ultrasound water indentation system. The dashed rectangles indicated the regions used for the plot of modulus profiles in Fig. 8.

the contrast of the modulus image. Fig. 6 shows the strain and corresponding modulus profiles across the selected horizontal zones of Fig. 5(c) and (f), as indicated by the dashed lines. Each value in Fig. 6 represents the mean of the data within the 0.6-mm-wide vertical region and the error bar indicates the SD of these data.

Fig. 7 shows the modulus images obtained from two independent scan sequences on the same phantom under the approximately same indentation level. Both of the images were obtained under the indentation pressure at 15.5 ± 2.8 kPa. As shown in Fig. 8, the modulus profiles obtained from the modulus images are identical within the measurement standard deviation (SD). Moreover, the correlation coefficient value of these two

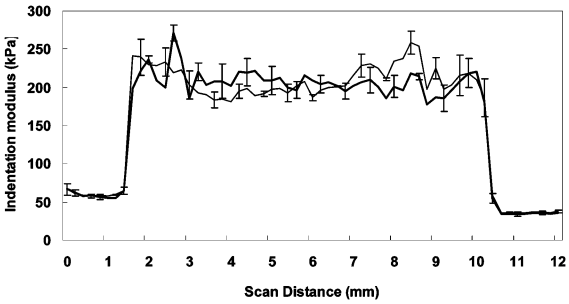

Fig. 8. Average modulus profile taken from the modulus images of Fig. 7(a) (the solid thin line) and Fig. 7(b) (the solid thick line). The error bar was plotted once per three points for a clearer view and indicated the modulus variation across the 0.4-mm-wide region around the center, which was indicated by the dashed rectangles in Fig. 7.

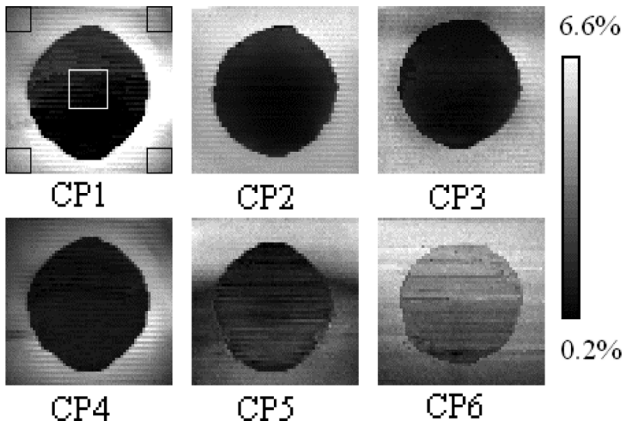

Fig. 9. Strain images obtained from the six phantoms with different inclusion/background modulus contrast. The pressure level to obtain these results was 14.5 ± 2.2 kPa.

modulus images was $r = 0.92$, indicating a high similarity between the two images. This demonstrated a good reproducibility of the modulus imaging using the ultrasound water indentation system.

Fig. 9 shows the six strain images obtained from the six different phantoms with varying inclusion/background modulus contrast at a pressure level of 14.5 ± 2.2 kPa. Fig. 10 shows the corresponding modulus images of CP1 to CP6. The modulus contrast was measured by estimating the average modulus of the inclusion and that of the background material. As the scan area was typically 12 mm $\times$ 12 mm and the inclusion size was 8 mm, the average modulus of the inclusion was obtained from a region of interest (ROI) of 3 mm $\times$ 3 mm at the center of the inclusion and the average modulus of the background was obtained from the average modulus in four ROIs (2 mm $\times$ 2 mm) at the four corners of the modulus image. The selection of ROIs was based on the criteria that the sites around the connective regions between the stiff and soft materials should not be included. The measured moduli of both inclusion and background materials were compared with their actual values obtained from the uniaxial compression tests. Fig. 11 shows the relationship between these two sets of modulus. The high correlation coefficient ($r = 0.99$) indicated a very good agreement between them, though some differences between the absolute

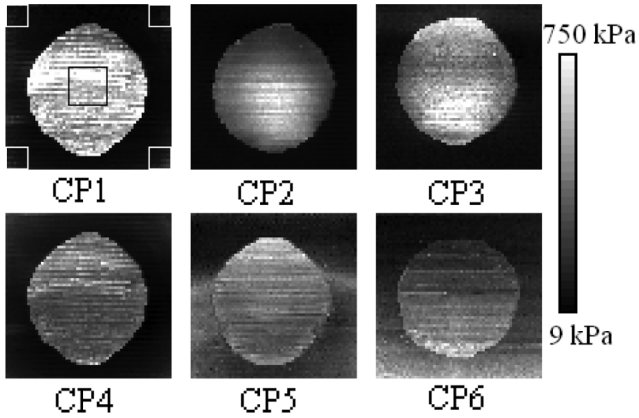

Fig. 10. Modulus images of phantoms CP1–CP6 using a water jet pressure level of 14.5 ± 2.2 kPa. The diameter of the cylindrical stiff inclusion was 8 mm and the scanning area was 12 mm $\times$ 12 mm. All images are displayed using the same dynamic range. The measured modulus contrast was 9.61, 8.96, 7.71, 3.95, 1.32, and 0.10 dB for phantom CP1 to CP6, respectively. The rectangles marked in the center of the inclusion and four corners of background of the modulus image of phantom CP1 indicated the regions used to calculate the modulus of the inclusion and background, respectively.

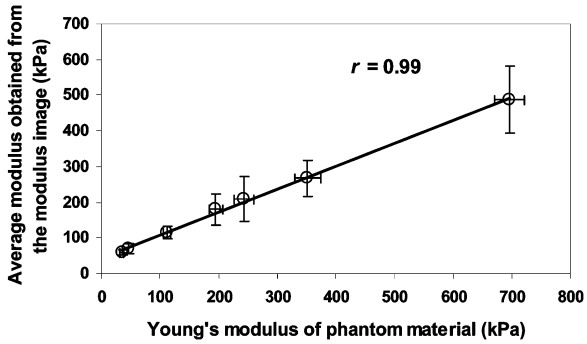

Fig. 11. The correlation between the moduli of the phantom materials determined using the water jet indentation and those measured using the uniaxial compression. The error bar indicates the SD of the measurements.

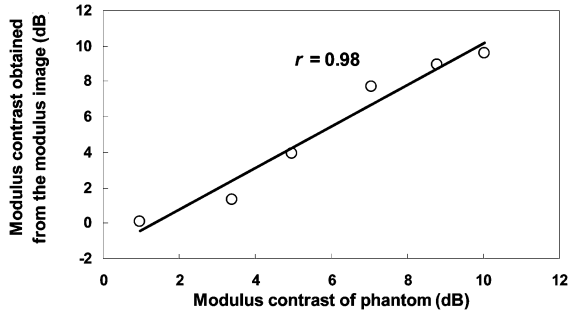

Fig. 12. The measured modulus contrasts of phantoms CP1–CP6 were compared to the corresponding actual modulus contrasts obtained from the uniaxial compression test.

values were noted. Fig. 12 is the correlation between the measured modulus contrast values and those obtained using the uniaxial compression tests. A good correlation was also found with a correlation coefficient ratio $r = 0.98$.

IV. Discussion

In this paper, we reported a new ultrasound water indentation system, which used a water jet as a "soft" indenter, for the

purpose of modulus imaging. Water jets have been widely used in the aerospace industry for several decades as they can provide noncontact coupling of ultrasound from the transducers to the test samples over a distance. In our previous study, the ultrasound water indentation system had been proved effective to measure the stiffness of silicone phantoms at a single point [51]. Compared with those contact indentation instruments, the ultrasound water indentation system appeared to be easily used to conduct C-scans for the sample, under different pressure levels of the water jet. By recording the water pressure and ultrasound signal simultaneously at each indentation site, the local stiffness ratio could be obtained from the indentation force, the local deformation and the original tissue thickness. The effective modulus image could be, thus, constructed. In this study, the phantoms with a symmetrical structure were used. The modulus contrast of the phantoms ranged from 0.97 to 10.02 dB, and a sharp transition of the modulus was assumed at the inclusion/background interface. As demonstrated in this study, the modulus images obtained using the new water indentation system could be used to effectively identify the stiff inclusions. The modulus contrasts obtained from the modulus image agreed very well with those measured using the uniaxial compression tests. The reproducibility of the modulus imaging was good with the correlation coefficient of 0.92 for the two modulus images obtained by two independent C-scans under the same pressure level. The new system showed its potential to obtain the modulus image of soft tissues with different modulus contrast *in vivo*, when the surface of the tissue is accessible. Obviously, many challenges need to be overcome before this water jet indentation method can be used *in vivo*, such as sterilization, collection of the ejected water or saline, miniaturization of the scanning mechanism, etc.

The spatial resolution of the measurements depended on the cross-sectional size and shape of the indenter, the ultrasound transducer parameters including frequency and beam width, as well as the connectivity between the stiff and soft region. In this study, we used a simple geometry of the phantom containing a uniform cylindrical stiff inclusion. For the modulus imaging experiments, a sharp transition of the modulus was assumed at the inclusion/background interface. The distance over which the transition occurred from 10% to 90% of the modulus values between a stiff and a soft region was estimated as the spatial resolution of the system [54]. For the current ultrasound water indentation system with a water jet indenter of 1.94 mm in diameter and an ultrasound frequency of 20 MHz, the spatial resolution estimated from the modulus profiles was approximately 0.4 mm. The spatial resolution could be further improved by increasing the ultrasound frequency and reducing the beam width [55].

The contrast resolution of the measurement using this ultrasound water indentation system is related to its ability to differentiate samples having different values of modulus E. If the modulus contrast was defined as the smallest difference of the modulus E between the two samples that was statistically significant, the contrast could be obtained from a statistical analysis using a 95% as 4σ confidence interval by assuming a normal distribution of the measured modulus E values [56]. For a σ value of 1.68 kPa computed from 35 independent measurements, the contrast resolution was expected to be 6.7 kPa at a 0.05 level of significance. This contrast resolution may satisfy the modulus imaging of most soft tissues [57].

In the current system, the water jet not only served as the indenter but also the coupling medium for the propagation of the ultrasound beam. A squirter may produce some disturbing reflections at the contact point following the front surface reflection, even when the water jet was smooth. These reflections could make the ultrasound reflection signal difficult to analyze. It was solved by selecting a suitable diameter of the squirter and focused beam width. Although the C-scan system that we used could be translated at a speed up to 500 $\mathrm{mm \cdot s^{-1}}$, the scan speed must be kept at a level that would not induce any water turbulence, which might introduce noise and affect the reliability of the test. Further investigations are required to study the optimized scanning speed for the water jet indentation.

In this study, we assumed that the phantoms had linear elastic material properties under the applied small deformation, and both inclusions and backgrounds were assumed to be homogeneous according to their fabrication procedures. However, the modulus images obtained from the water jet indentation method did not appear uniform, particularly when the applied pressure was relatively larger. One possible explanation might be that the inclusion materials around the background-inclusion interface may appear to be softer in comparison with those in the middle portion, as the inclusion materials near the interface was less confined, or confined with softer materials. Thus, the middle portion would have a relatively smaller strain and subsequently a larger modulus could be derived even the applied pressure was the same. This boundary effect would increase with the increase of the applied force or the applied deformation. That is why we noted that the inclusion became more inhomogeneous as the increase of the pressure level. This artifact could be avoided if we had a mechanical model for the whole phantom with the boundary conditions included. Further investigations towards this direction are required in the future.

We used an indentation model previously developed for a flat cylindrical indenter to extract the modulus from pressure-deformation data [6], assuming that the water jet maintained its initial diameter and cylindrical shape after hitting the phantom surface under the small deformation. This might be too simplified in modeling the interaction between the water jet and phantom as the nonlinear behaviors of fluids would occur during the deformation of the phantom, particularly for a large deformation. This should be one of the reasons why the absolute value of the modulus obtained using the water indentation was different from that measured using the uniaxial compression tests for the same phantom material (Fig. 11). The absolute value of the modulus obtained using the water jet indentation can also be affected by the Poisson's ratio of the phantom materials [6], [7]. In spite of these effects, a good linear relationship was observed between the modulus of the phantoms obtained by the two methods. In addition, it is required that the lateral dimension of the sample should be 3 times larger than the indenter diameter according to the indentation model using cylindrical indenters [6], [53]. This requirement might not always be fulfilled for the real tissues so that the lateral boundary conditions should be considered in the indentation model. Further investigation will be continued to extract the absolute modulus of the phantom more accurately

by considering the effects of the Poisson's ratio, the boundary conditions, and the complicated interaction between the water jet and the phantom surface.

Furthermore, it is well known that body tissues have nonlinear and viscoelastic material properties [3] and the deformation during indentation test may also be larger than that used in this study. Therefore, future studies are needed to explore more accurate modeling for the interaction between the water jet and the tissues with different mechanical properties and under different indentation deformations.

V. Conclusion

In summary, the ultrasound water indentation system shows its ability to map the compressive modulus distribution of the phantoms, even with small modulus contrasts. Further studies are required to investigate more accurate descriptions of the interaction between the water jet and the tissues. Its performance for the measurement of various biological tissues should also be further tested by using real tissue specimens. This system may have potential applications for the assessment of different tissues. With further improvements of the system and better understanding about the water jet-tissue interaction, we expect that the water indentation approach could be potentially used to image the modulus distribution of body tissues for clinical assessment and diagnosis, including skin tumor formation, tissue scarring, articular cartilage degeneration (together with arthroscopy), etc. For these potential applications, clinically used sterilized saline pump can be used to provide water jet and proper mechanisms should be used to collect the ejected saline. With further development, his technique might also be potentially employed to perform indentation tests on small specimens at microscopic levels for biological tissues and other materials, such as small animal tissues, bioengineered tissues, semiconductor materials, thin films, etc., where nanoindentation is widely used.

References

[1] M. Mridha and S. Odman, "Noninvasive method for assessment of subcutaneous edema," *Med. Biol. Eng. Comput.*, vol. 24, pp. 393–398, 1986.

[2] B. S. Garra, E. I. Cespedes, J. Ophir, S. R. Spratt, R. A. Zuurbier, C. M. Magnant, and M. F. Pennanen, "Elastography of breast lesions: Initial clinic results," *Radiology*, vol. 202, pp. 79–86, 1997.

[3] Y. C. Fung, *Biomechanical Properties of Living Tissues*. New York: Springer-Verlag, 1981.

[4] V. C. Mow and W. C. Hayes, *Basic Orthopaedic Biomechanics*, 2nd ed. Philadelphia, PA: Lippincott-Raven, 1997.

[5] N. E. Waters, "The indentation of thin rubber sheets by spherical indentors," *Br. J. Appl. Phys.*, vol. 16, pp. 557–563, 1965.

[6] W. C. Hayes, G. Herrmann, L. F. Mockros, and L. M. Keer, "A mathematical analysis for indentation tests of articular cartilage," *J. Biomech.*, vol. 5, pp. 541–551, 1972.

[7] A. F. Mak, W. M. Lai, and V. C. Mow, "Biphasic indentation of articular-cartilage. 1. Theoretical analysis," *J. Biomech.*, vol. 20, pp. 703–714, 1987.

[8] V. C. Mow, M. C. Gibbs, W. M. Lai, W. B. Zhu, and K. A. Athanasiou, "Biphasic indentation of articular-cartilage.2. A numerical algorithm and an experimental-study," *J. Biomech.*, vol. 22, pp. 853–861, 1989.

[9] D. Chicot, I. Hage, P. Demarecaux, and J. Lesage, "Elastic properties determination from indentation tests," *Surf. Coat. Tech.*, vol. 81, pp. 269–274, 1996.

[10] W. P. Yu and J. P. Blanchard, "An elastic-plastic indentation model and its solutions," *J. Mater. Res.*, vol. 11, pp. 2358–2367, 1996.

[11] M. Sakamoto, G. A. Li, T. Hara, and E. Y. S. Chao, "A new method for theoretical analysis of static indentation test," *J. Biomech.*, vol. 29, pp. 679–685, 1996.

[12] M. A. Haider and M. H. Holmes, "A mathematical approximation for the solution of a static indentation test," *J. Biomech.*, vol. 30, pp. 747–751, 1997.

[13] L. S. Wilson and D. E. Robinson, "Ultrasonic measurement of small displacements and deformations of tissue," *Ultrason. Imag.*, vol. 4, pp. 71–82, 1982.

[14] Y. P. Zheng and A. F. T. Mak, "An ultrasound indentation system for biomechanical properties assessment of soft tissues *in vivo*," *IEEE Trans. Biomed. Eng.*, vol. 43, no. 9, pp. 912–918, Sep. 1996.

[15] T. C. Hsu, C. L. Wang, W. C. Tsai, J. K. Kuo, and F. T. Tang, "Comparison of the mechanical properties of the heel pad between young and elderly adults," *Arch. Phys. Med. Rehabil.*, vol. 79, pp. 1101–1104, 1998.

[16] C. Adam, F. Eckstein, S. Milz, E. Schulte, C. Becker, and R. Putz, "The distribution of cartilage thickness in the knee-joints of old-aged individuals—Measurement by A-mode ultrasound," *Clin. Biomech.*, vol. 13, pp. 1–10, 1998.

[17] G. N. Kawchuk, O. R. Fauvel, and J. Dmowski, "Ultrasonic quantification of osseous displacements resulting from skin surface indentation loading of bovine para-spinal tissue," *Clin. Biomech.*, vol. 15, pp. 228–233, 2000.

[18] J. K. F. Suh, I. Youn, and F. H. Fu, "An in situ calibration of an ultrasound transducer: A potential application for an ultrasonic indentation test of articular cartilage," *J. Biomech.*, vol. 34, pp. 1347–1353, 2001.

[19] M. S. Laasanen *et al.*, "Novel mechano-acoustic technique and instrument for diagnosis of cartilage degeneration," *Physiol. Meas.*, vol. 23, pp. 491–503, 2002.

[20] L. H. Han, J. A. Noble, and M. Burcher, "A novel ultrasound indentation system for measuring biomechanical properties of *in vivo* soft tissue," *Ultrasound Med. Biol.*, vol. 29, pp. 813–823, 2003.

[21] Y. P. Zheng and A. F. T. Mak, "Extraction of quasilinear viscoelastic parameters for lower limb soft tissues from manual indentation experiment," *J. Biomech. Eng.—Trans. ASME*, vol. 121, pp. 330–339, 1999.

[22] ——, "Effective elastic properties for lower limb soft tissues from manual indentation experiment," *IEEE Trans. Rehabil. Eng.*, vol. 7, no. 3, pp. 257–267, Sep 1999.

[23] Y. P. Zheng, A. F. T. Mak, and B. Lue, "Objective assessment of limb tissue elasticity: Development of a manual indentation procedure," *J. Rehabil. Res. Dev.*, vol. 36, pp. 71–85, 1999.

[24] Y. P. Zheng, Y. K. C. Choi, K. Wong, S. Chan, and A. F. T. Mak, "Biomechanical assessment of plantar foot tissue in diabetic patients using an ultrasound indentation system," *Ultrasound Med. Biol.*, vol. 26, pp. 451–456, 2000.

[25] Y. P. Zheng, S. F. Leung, and A. F. T. Mak, "Assessment of neck tissue fibrosis using an ultrasound palpation system: A feasibility study," *Med. Biol. Eng. Comput.*, vol. 38, pp. 497–502, 2000.

[26] S. F. Leung *et al.*, "Quantitative measurement of post-irradiation neck fibrosis based on the young modulus: Description of a new method and clinical results," *Cancer*, vol. 95, pp. 656–662, 2002.

[27] Y. P. Huang, Y. P. Zheng, and S. F. Leung, "Quasi-linear viscoelastic properties of fibrotic neck tissues obtained from ultrasound indentation tests *in vivo*," *Clin. Biomech.*, vol. 20, pp. 145–154, 2005.

[28] G. N. Kawchuk, O. R. Fauvel, and J. Dmowski, "Ultrasound indentation: A procedure for the noninvasive quantification of force-displacement properties of the lumber spine," *J. Manip. Physiol. Ther.*, vol. 24, pp. 149–156, 2001.

[29] Y. P. Zheng, A. F. T. Mak, K. P. Lau, and L. Qin, "An ultrasonic measurement for *in vitro* depth-dependent equilibrium strains of articular cartilage in compression," *Phys. Med. Biol.*, vol. 47, pp. 3165–3180, 2002.

[30] K. W. Hollman *et al.*, "Strain imaging of corneal tissue with an ultrasound elasticity microscope," *Cornea*, vol. 21, pp. 68–73, 2002.

[31] Y. P. Zheng *et al.*, "High resolution ultrasound elastomicroscopy imaging of soft tissues: System development and feasibility," *Phys. Med. Biol.*, vol. 49, pp. 3925–3938, 2004.

[32] W. M. Vannah, D. M. Drvaric, J. A. Hastings, J. A. Stand, and D. M. Harning, "A method of residual limb stiffness distribution measurement," *J. Rehab. Res. Dev.*, vol. 36, pp. 1–7, 1999.

[33] R. C. Appleyard, M. V. Swain, S. Khanna, and G. A. C. Murrell, "The accuracy and reliability of a novel handheld dynamic indentation probe for analysing articular cartilage," *Phys. Med. Biol.*, vol. 46, pp. 541–550, 2001.

[34] W. C. Oliver and G. M. Pharr, "An improved technique for determining hardness and elastic modulus using load and displacement sensing indentation experiments," *J. Mater. Res.*, vol. 7, pp. 1564–1583, 1992.

[35] L. H. Guo, X. Guo, Y. Leng, J. C. Y. Cheng, and X. D. Zhang, "Nanoindenation study of interfaces between calcium phosphate and bone in an animal spinal fusion model," *J. Biomed. Mater. Res.*, vol. 54, pp. 554–559, 2001.
[36] J. Ophir, I. Cespedes, H. Ponnekanti, Y. Yazdi, and X. Li, "Elastography: A quantitative method for imaging the elasticity of biological tissues," *Ultrason. Imag.*, vol. 13, pp. 111–134, 1991.
[37] I. Cespedes and J. Ophir, "Reduction of image noise in elastography," *Ultrason. Imag.*, vol. 15, pp. 89–102, 1993.
[38] J. Ophir, S. K. Alam, B. Garra, F. Kallel, E. Konofagou, T. Krouskop, and T. Varghese, "Elastography: Ultrasonic estimation and imaging of the elastic properties of tissues," *J. Eng. Med.*, vol. 213, no. H3, pp. 203–233, 1999.
[39] S. F. Levinson, M. Shinagawa, and T. Sato, "Sonoelasticity determination of human skeletal muscle elasticity," *J. Biomech.*, vol. 28, pp. 1145–1154, 1995.
[40] A. P. G. Hoeks, P. J. Brands, J. M. Willingers, and R. S. Reneman, "Non-invasive measurement of mechanical properties of arteries in health and disease," *Proc. Inst. Mech. Eng.*, vol. 213, pp. 195–202, 1999.
[41] S. Y. Emelianov, M. A. Lubinski, A. R. Skovoroda, R. Q. Erkamp, S. F. Leavey, R. C. Wiggins, and M. O'Donnell, "Reconstructive ultrasound elasticity imaging for renal transplant diagnosis: Kidney *ex vivo* results," *Ultrason. Imag.*, vol. 22, pp. 178–194, 2000.
[42] T. A. Krouskop, D. R. Dougherty, and F. S. Vinson, "A pulsed doppler ultrasonic system for making noninvasive measurement of the mechanical properties of soft tissue," *J. Rehabil. Res. Biol.*, vol. 14, pp. 1–8, 1987.
[43] R. M. Lerner, S. R. Huang, and K. J. Parker, "Sonoelasticity images derived from ultrasound signals in mechanically vibrated tissues," *Ultrasound Med. Biol.*, vol. 16, pp. 231–239, 1990.
[44] Y. Yamakoshi, J. Sato, and T. Sato, "Ultrasonic imaging of internal vibration of soft tissue under forced vibration," *IEEE Trans. Ultrason. Ferroelect. Freq. Contr.*, vol. 37, no. 2, pp. 45–53, Mar. 1990.
[45] L. Sandrin, M. Tanter, S. Catheline, and M. Fink, "Shear modulus imaging with 2-D transient elastography," *IEEE Trans. Ultrason. Ferroelect. Freq. Contr.*, vol. 49, no. 4, pp. 426–435, Apr. 2002.
[46] M. Fatemi and J. F. Greenleaf, "Ultrasound stimulated vibro-acoustic spectrography," *Science*, vol. 280, pp. 82–85, 1998.
[47] K. Nightingale, M. S. Soo, and G. Trahey, "Acoustic radiation force impulse imaging: *In vivo* demonstration of clinical feasibility," *Ultrasound Med. Biol.*, vol. 28, pp. 227–235, 2002.
[48] S. Chen, M. Fatemi, and J. F. Greenleaf, "Remote measurement of material properties from radiation force induced vibration of an embedded sphere," *J. Acoust. Soc. Am.*, vol. 112, pp. 884–889, 2002.
[49] A. S. Birks and R. E. Green, *Nondestructive Testing Handbook: Ultrasonic Testing*. Columbus, OH: Am. Soc. Nondestructive Testing, 1991.
[50] M. Lasser, B. Lasser, J. Kula, and G. Rohrer, "On-line, large area ultrasonic imaging for composite manufacturing," in *Am. Soc. Nondestructive Testing Conf.*, Phoenix, AZ, Oct. 11–15, 1999.
[51] M. H. Lu, Y. P. Zheng, and Q. H. Huang, "A novel noncontact ultrasound indentation system for measurement of tissue material properties using water jet compression," *Ultrasound Med. Biol.*, vol. 31, pp. 817–826, 2005.
[52] T. J. Hall, M. Bilgen, M. F. Insana, and T. A. Krouskop, "Phantom materials for elastography," *IEEE Trans. Ultrason. Ferroelect. Freq. Contr.*, vol. 44, no. 6, pp. 1355–1365, Nov. 1997.
[53] P. C. Galbraith and J. T. Bryant, "Effect of grid dimensions on finite element models of an articular surface," *J. Biomech.*, vol. 22, pp. 385–393, 1989.
[54] S. Srinivasan, T. Krouskop, and J. Ophir, "Comparing elastographic strain images with modulus images obtained using nanoindentation: Preliminary results using phantoms and tissue samples," *Ultrasound Med. Biol.*, vol. 30, pp. 329–343, 2004.
[55] F. S. Foster, C. J. Pavlin, K. A. Harasiewicz, D. A. Christopher, and D. H. Turnbull, "Advances in ultrasound biomicroscopy," *Ultrasound Med. Biol.*, vol. 26, pp. 1–27, 2000.
[56] J. S. Bendat and A. G. Piersol, *Random Data: Analysis and Measurement*, 2nd ed. New York: Wiley, 1986.
[57] T. A. Krouskop, T. M. Wheeler, F. Kallel, B. S. Garra, and T. Hall, "The elastic moduli of breast and prostate tissues under compression," *Ultrason. Imag.*, vol. 20, pp. 260–274, 1998.

Min-Hua Lu (S'05–M'06) was born in Jiangsu Province of China in April, 1977. She received the B.E. degree in electronic engineering and information science from the University of Science and Technology of China, He Fei, China, in June, 2001. She is currently working towards the Ph.D. degree in the Department of Health Technology and Informatics, the Hong Kong Polytechnic University, Hong Kong.

Her research interest is the measurement and imaging of tissue mechanical properties using ultrasound or other modalities, such as optical coherence tomography.

Yong-Ping Zheng (S'95–A'98–M'99–SM'06) received the B.Sc. degree in electronics and information engineering and M.Eng. in ultrasound instrumentation from the University of Science and Technology of China, He Fei. He received the Ph.D. degree in biomedical engineering from the Hong Kong Polytechnic University (PolyU), Hong Kong, in 1997.

After a postdoctoral fellowship in acoustic microscope and nonlinear acoustics at the University of Windsor, Windsor, ON, Canada, he joined PolyU as an Assistant Professor in 2001 and was promoted to Associate Professor in May 2005. His main research interests include ultrasound elasticity imaging and measurement, three-dimensional ultrasound imaging, ultrasonic characterization of articular cartilage, and ultrasound instrumentation. He and his co-workers hold three US patents, and have 9 patents filed (US and China) since 2002, mainly in the field of biomedical ultrasound.

Qing-Hua Huang (S'05–M'06) was born in Heilongjiang, China, in November 1976. He received the B.E. and M.E. degrees in automatic control and pattern recognition, respectively, both from the University of Science and Technology of China in 1999 and 2002. He received the Ph.D. degree in biomedical engineering in July, 2006, at the Hong Kong Polytechnic University (PolyU).

He joined the rehabilitation engineering center of the PolyU as a Research Assistant in 2002, and is now a Research Associate with the Department of Health Technology and Informatics at the same university. His research interests include three–dimensional ultrasound imaging, medical image analysis, and intelligent computation for biomedical signals.